RESEARCH

The effect of absent blood flow on the zebrafish cerebral and trunk vasculature

Elisabeth Kugler[1,2,3,4], **Ryan Snodgrass**[1,2], **George Bowley**[1,2], **Karen Plant**[1,2], **Jovana Serbanovic-Canic**[1,2], **Noémie Hamilton**[1,2], **Paul C Evans**[1,2,3], **Timothy Chico**[1,2] and **Paul Armitage**[1,3]

[1]Department of Infection, Immunity and Cardiovascular Disease, University of Sheffield, Medical School, Sheffield, UK
[2]The Bateson Centre, Firth Court, University of Sheffield, Western Bank, Sheffield, UK
[3]Insigneo Institute for in silico Medicine, Sheffield, UK
[4]Institute of Ophthalmology, Faculty of Brain Sciences, University College London, London, UK

Correspondence should be addressed to E Kugler: e.kugler@ucl.ac.uk

Abstract

The role of blood flow in vascular development is complex and context-dependent. In this study, we quantify the effect of the lack of blood flow on embryonic vascular development on two vascular beds, namely the cerebral and trunk vasculature in zebrafish. We perform this by analysing vascular topology, endothelial cell (EC) number, EC distribution, apoptosis, and inflammatory response in animals with normal blood flow or absent blood flow. We find that absent blood flow reduced vascular area and EC number significantly in both examined vascular beds, but the effect is more severe in the cerebral vasculature, and severity increases over time. Absent blood flow leads to an increase in non-EC-specific apoptosis without increasing tissue inflammation, as quantified by cerebral immune cell numbers and nitric oxide. Similarly, while stereotypic vascular patterning in the trunk is maintained, intra-cerebral vessels show altered patterning, which is likely to be due to vessels failing to initiate effective fusion and anastomosis rather than sprouting or path-seeking. In conclusion, blood flow is essential for cellular survival in both the trunk and cerebral vasculature, but particularly intra-cerebral vessels are affected by the lack of blood flow, suggesting that responses to blood flow differ between these two vascular beds.

Introduction

Endothelial cells (ECs) perform multiple functions during normal physiology including wound healing, tissue regeneration, immune response, menstruation, and pregnancy (1, 2, 3). Cerebral EC dysfunction is associated with neurodegenerative diseases, arteriovenous malformations, aneurysms, and stroke (4, 5). Increasing evidence suggests ECs display different molecular and functional properties according to their anatomical site, such as the cerebral or trunk vessels (6, 7, 8, 9, 10). This highlights the importance of studying the responses of multiple vascular in development and territories to experimental manipulations.

Zebrafish embryos are a frequently used model to study vascular development and disease (11, 12, 13). Fluorescent transgenic reporter lines allow cellular and sub-cellular visualization *in vivo* (14). Advanced microscopy, such as light sheet fluorescence microscopy (LSFM), acquires vascular information in great anatomical depth and over prolonged periods of time (15), allowing data acquisition to be rich in information and detail. Zebrafish embryonic

transparency allows non-invasive and *in vivo* studies of different vascular beds in the same animal.

After 24 h post-fertilization (hpf), the zebrafish basic body plan is established and cardiac contraction starts. Within this timeframe, vasculogenesis forms the primary vessels (16, 17). Blood flow plays an important role in processes, such as EC polarization, vascular lumenization, pruning, and cardiac trabeculation (18, 19, 20, 21, 22, 23, 24), and directly impacts vascular architecture (25). Zebrafish embryos can survive for 7 days post fertilization (dpf) without blood flow via oxygen diffusion due to their small size (13, 26). This makes them well suited to examine the role of blood flow on vasculogenesis and angiogenesis.

One approach to study the effect of absent blood flow in zebrafish is the knockdown of cardiac troponin T2A (*tnnt2a*) using antisense morpholino oligonucleotides (MO). This prevents cardiac contraction and thus blood flow (27, 28). Contrary to recent debates on MO phenocopying mutant phenotypes, the *tnnt2a* MO phenocopies the silent heart (*sih*) mutation (28), making it a widely used MO-based approach to study the lack of blood flow. Additionally, a control MO group accounts for injection-induced developmental delays (29). Previous studies used this MO-based method to study the impact of blood flow on specific cerebral (30, 31) and trunk vessels (32), showing that EC numbers are reduced in the trunk when blood flow is absent (32, 33).

Even though these studies have provided invaluable insights into the role of blood flow, important questions remain unanswered about the role of blood flow in vascular development. These include whether absent blood flow has the same effects in different vascular beds, whether vessels of different identities respond differently, which steps of vasculature formation are altered, and whether effect sizes of absent blood flow differ in magnitude over time.

To examine these questions. we here use LSFM 3D *in vivo* imaging of the cerebral and trunk vasculature of 2–5dpf zebrafish embryos with and without blood flow induced by *tnnt2a* knockdown. Our results show that even though the gross vascular responses to blood flow are comparable in different territories, some differences between anatomical sites exist, suggesting vascular territories exhibit differential sensitivity to absent blood flow.

Materials and methods

Zebrafish husbandry

Experiments were performed according to the rules and guidelines of institutional and UK Home Office

regulations under the Home Office Project Licence 70/8588 held by TC.

Maintenance of adult zebrafish was performed as described in standard husbandry protocols (34, 35). Embryos, obtained from controlled mating, were kept in E3 (5 mM NaCl, 0.17 mM KCl, 0.33 mM CaCl$_2$, 0.33 mM MgSO$_4$) medium buffer with methylene blue and staged according to Kimmel *et al.* (36). The following transgenic reporter lines were used: *Tg(kdrl:HRAS-mCherry)^{s916}* (37) visualizes EC membrane, *Tg(fli1a:eGFP)^{y1}* (14) visualizes EC cytosol, *Tg(flk1:nls-eGFP)^{zf109}* (38) visualizes EC nuclei, *Tg(mpx:GFP)^{i114}* (39) visualizes neutrophils, and *Tg(fms:GAL4.VP16)^{i186}*, *Tg(UAS-E1b:nfsB.mCherry)^{il149}* (40) visualizes macrophages. To assess cell death *in vivo*, we created the stable transgenic *Tg(secAnnexinV:mVenus)^{SH632}* in pDestCryaa:RFP, similar to (41) and the plasmid cloning of (42).

Morpholino injection

Development of functional heart contraction was inhibited via injection of *tnnt2a* ATG morpholino (1.56 ng final concentration), as described in (27, 28) (sequence 5'-CATGTTTGCTCT GATCTGACACGCA-3'). Control morpholino injections (5'-CCTCTTACCTCAGTTATTTATA-3'; no target sequence and little/no biological activity; Genetools, LLC) were performed with the above final concentration to study off-target effects of injections. Injections were conducted at a one-cell stage using phenol red as an injection tracer.

Chemical and histological stains

In vivo visualization of cell death was performed using 2 µg/mL solution of Acridine Orange (Sigma) in 1X E3 for 2 h in 3dpf embryos, followed by three washes in E3 before image acquisition (43).

In vivo visualization of inflammation via nitric oxide (NO) (44) was performed using 2.5 µM DAF-FM-DA (Molecular Probes; D23844) (45) for 6 h in 3dpf embryos. DMSO control was performed at the same concentration and duration.

Image acquisition settings and properties

Anaesthetized embryos were embedded in 2% LMP-agarose with 0.01% Tricaine in E3 (MS-222, Sigma). Data acquisition of the cranial and trunk vasculature was performed using a Zeiss Z.1 light sheet microscope, Plan-Apochromat 20×/1.0 Corr nd = 1.38 objective, dual-side

illumination with online fusion, activated Pivot Scan, image acquisition chamber incubation at 28°C, and a scientific complementary metal-oxide-semiconductor (sCMOS) detection unit. The properties of acquired data were as follows: 16 bit image depth, 1920 × 1920 × 400–600 voxel (x,y,z; approximate voxel size of 0.33 × 0.33 × 0.5 μm, respectively). Multicolour images in double-transgenic embryos were acquired in sequential mode.

Image analysis

As *tnnt2a* can develop considerable oedema, we ensured comparability between samples by standardized image acquisition from the dorsal view, including the most dorsal vessel the dorsal longitudinal vein (DLV) to the more ventral basilar artery (BA; Supplementary Fig. 3A, see section on supplementary materials given at the end of this article). For image analysis, ROI selection was performed as previously described (Supplementary Fig. 9B) (46).

Automatic nuclei detection

To remove salt-and-pepper noise (47), a 6-by-6 neighbourhood median filter (48) was applied, while background removal was achieved with the rolling ball algorithm with size 200 (49). Following, 2D maximum intensity projection, and detection of local noise maxima using Fiji Software (50, 51). The Voronoi diagram was established following Otsu thresholding (52). Nuclei nearest neighbour distance (NND) was quantified in MIPs following pre-processing as above and Otsu thresholding, using the Fiji NND plugin (https://icme.hpc.msstate. edu/mediawiki/index.php/Nearest_Neighbor_Distances_ Calculation_with_ImageJ.html).

Signal intensities

Signal intensity measurement of Acridine Orange and DAF-FM was conducted by creating 3D vascular masks following Sato filter for vascular enhancement and Otsu thresholding segmentation as previously described (46, 53, 54). Signal mean was quantified in ROIs in 2D MIPs. The signal-to-noise (SNR) ratio was quantified as the mean signal in ROI divided by the mean signal of the background (ROI placed outside the fish with a size of 10 × 10 μm). Acridine orange foci were detected in ROI following 2D median filtering using the detection of maxima with intensity over 10.

Manual analysis

All analysis was performed using Fiji (51).

Diameter of basilar artery (BA) was measured approximately 30 μm before bifurcating into posterior (caudal) communicating segments (PCS).

Posterior cerebral vein (PCeV) was measured approximately 20 μm before turning dorsally.

Posterior cardinal vein (PCV) and dorsal aorta (DA) diameters were measured above the cloaca, with three measurement points each in the same animal.

Intersegmental vessel (ISV) lengths of arterial (aISVs) and venous (vISVs) were measured above the cloaca, with three measurement points of the same vessels each in the same animal.

Vessel-specific nuclei measurements were conducted manually. First, nuclei were counted in aISVs and vISVs closest to the cloaca. Secondly, nuclei in the PCeV and BA were measured in an 80 μm long ROI positioned from the posterior end of the PCeV.

CtA sprouting and connectivity to BA were measured manually from the left PHBC.

Immune cells

Intracranial macrophages and neutrophils were quantified manually in 3D after ROI selection of the dorsal cerebral vasculature.

Availability of data and the code

Data and code will be made available upon request.

Statistical analysis

Gaussian distribution conformation was evaluated using the D'Agostino-Pearson omnibus test (21). Statistical analysis was performed using one-way ANOVA or paired Students *t*-test in GraphPad Prism Version 7 (GraphPad Software). Statistical significance was represented as: $*P < 0.05$, $**P < 0.01$, $***P < 0.001$, $****P < 0.0001$. Graphs show mean values ± S.D. unless otherwise indicated. Image representation and visualization were done with Inkscape Version 0.48 (https://www.inkscape.org). Images were visualized as maximum intensity projections (MIPs). 3D rendering was performed using Arivis software (arivis AG, Munich, Germany).

Results

#### Cerebrovascular patterning is impaired by absent blood flow

We first examined whether cerebrovascular patterning is altered by lack of blood flow. Thus, we compared the

cerebral vascular morphology of uninjected controls (Fig. 1A, B, C and D), control MO (Fig. 1E, F, G and H), and *tnnt2a* MO-injected embryos (Fig. 1I, J, K and L). When examining the global morphology, *tnnt2a* MO showed pericardial oedema, eye oedema, smaller eyes, and abnormal body curvature, which became more severe over time (Supplementary Fig. 1). The *tnnt2a* morphants were smaller with overtly abnormal cerebral vasculature, with effects becoming more severe from 2 to 5dpf. Intra-cerebral vessels, especially in the midbrain, were most severely affected showing altered growth patterns and an overall reduction of cerebral size was observed (Fig. 1L, dotted line). The primary head sinus (PHS), which extends laterally to the otic vesicle (OV), was enlarged,

suggesting OV enlargement (Fig. 1L, filled arrowheads), while peripheral/perineural vessels, such as the primordial hindbrain channel (PHBC), formed relatively normally (Fig. 1L, unfilled arrowhead; schematic of cerebral vessels from 2 to 5dpf Supplementary Fig. 2). Our observations also confirm previous work in which vessels from the spinal cord and brain are still undergoing integration in the absence of blood flow (55).

We next examined the distribution of EC in these animals (Fig. 2). This also suggested that peripheral vessels were less severely affected by absent blood flow, for example, when comparing nuclei distribution in the middle cerebral vein (MCeV, Fig. 2, unfilled arrowhead) to central arteries (Fig. 2, black arrowhead). This was confirmed when examining Voronoi diagrams of EC nuclei distribution (Fig. 2M, N and O). Voronoi tessellation, overlapping nuclei images, aided the visualization of EC nuclei density/ distribution by partitioning MIPs into sub-regions based on nuclei position. Thus the Voronoi diagram lines and their colour indicate the spatial relationship of nuclei to each other, for example, larger tessellation and brighter colours show that a larger region is taken up by a nucleus. This showed EC distribution to be altered, particularly in the basilar artery (BA) or midbrain vessels.

This suggested that the effect of lack of blood flow becomes more severe over time and that central vessels are more impacted than peripheral vessels.
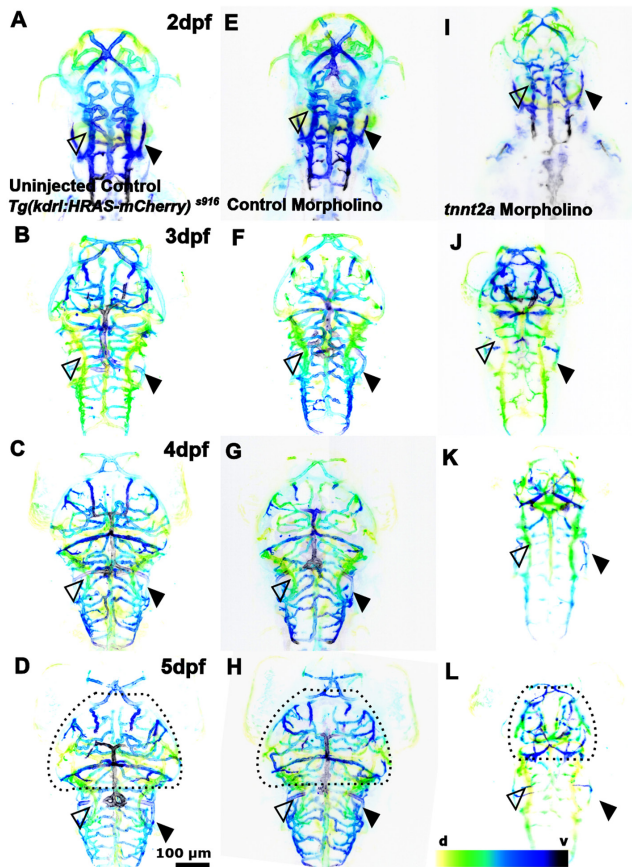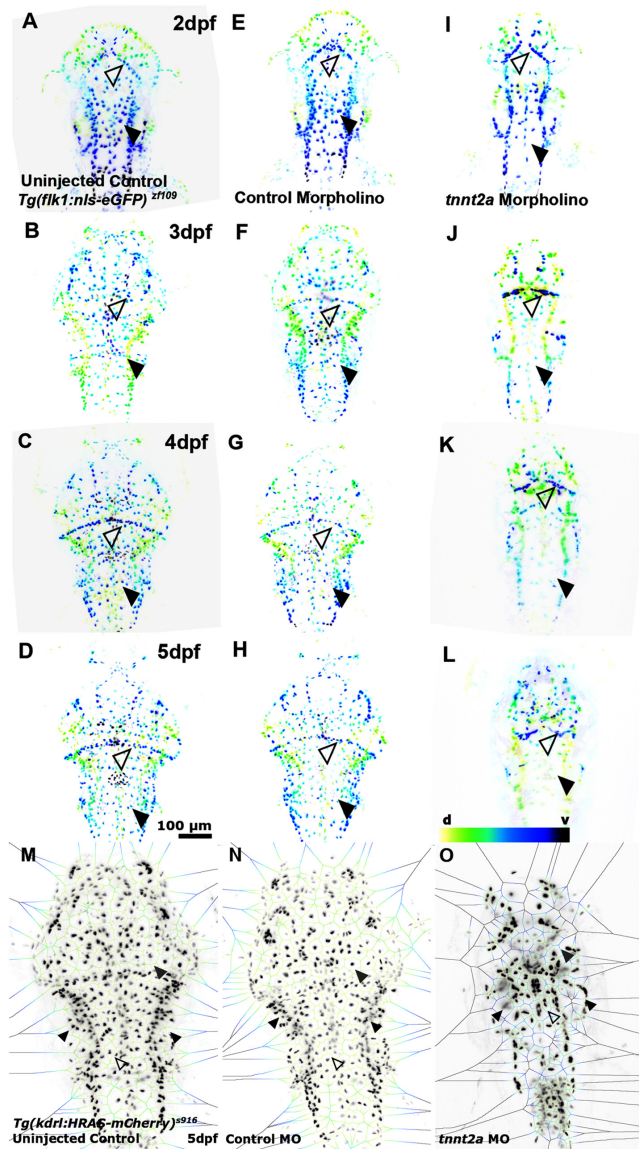

Figure 1
The effect of *tnnt2a* morpholino knockdown on cerebral vessel development. (A, B, C and D) Cerebral vasculature from 2 to 5dpf in *Tg(kdrl:HRAS-mCherry)^{s916}* uninjected animals. (E, F, G and H) Cerebral vasculature in control MO-injected animals. (I, J, K and L) Cerebral vasculature in *tnnt2a* MO injected animals (*n* = 7–10; two experimental repeats). The lack of blood flow in *tnnt2a* morphants perturbs vascular development and worsens over time. Comparison between treatment groups shows that the midbrain vasculature is severely affected in *tnnt2a* MO (dotted lines) and the PCV surrounding the OV is enlarged (filled arrowhead), while the PHBC appears normal (unfilled arrowhead; d – dorsal, v – ventral; representative images colour-coded by depth).

Vascular patterning in the trunk is preserved, but vascular morphology altered

We next examined vascular patterning in the trunk of the same animals to study whether the observed effects were conserved or different in these vascular beds (Fig. 3A, B, C, D, E, F, G, H, I, J, K and L). Vessels formed by vasculogenesis were observed and in contrast to the cerebral vessels, trunk vessel patterning was largely unaltered in the absence of flow. However, the morphology of the caudal vein plexus (CVP) was less defined upon lack of blood flow (Fig. 3, white arrowhead) and intussusceptive pillars were lacking (Fig. 3A′, E′ and I′). All our observations were consistent with previous studies that blood flow is required for plexus to caudal vein remodelling (56). Intussusception, and dorsal aorta (DA)-to-CVP segregation (57), but not intersegmental vessel (ISV) migration (17).

We next examined whether trunk EC numbers were changed. Examination of EC nuclei suggested EC numbers in the trunk were less severely impacted by lack of blood flow in comparison to cerebral vessels (Fig. 4), with EC
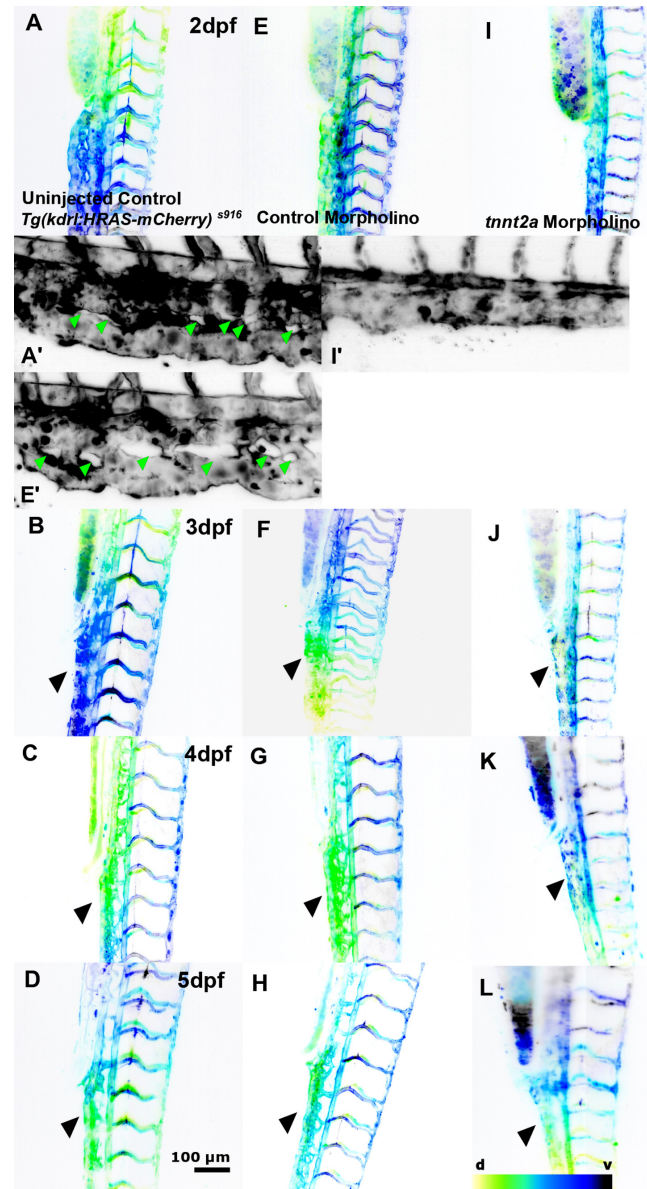
Figure 2

Lack of blood flow impacts cerebral EC number. (A, B, C and D) Cerebral EC nuclei from 2 to 5dpf in *Tg(flk1:nls-eGFP)*^zf109 uninjected control. (E, F, G and H) Cerebral EC nuclei in control MO. (I, J, K and L) Cerebral EC nuclei in *tnnt2a* MO (*n* = 7–10; two experimental repeats). Comparison of cerebral EC nuclei shows reduced cell numbers in *tnnt2a* MO with CtAs (filled arrowhead) being particularly affected (d – dorsal, v – ventral; representative images colour-coded by depth). (M, N and O) Voronoi (image partitioning based on nuclei position) diagrams of cerebral EC nuclei suggests nuclei numbers to be maintained in peripheral vessels such as the PHBC (white arrowheads), while EC density is reduced in the midbrain (grey arrowhead) and BA (unfilled arrowhead).

Figure 3

The effect of absent blood flow on trunk vessel development. (A, B, C and D) Trunk vasculature from 2 to 5dpf in *Tg(kdrl:HRAS-mCherry)*^s916 uninjected control. (E, F, G and H) Trunk vasculature in control MO (*n* = 7–10; two experimental repeats). (I, J, K and L) Trunk vasculature in *tnnt2a* MO. Topology of the trunk vasculature is established in the absence of flow, but morphology of the CV is severely altered (black arrowheads) and intussusceptions are lacking (green arrowhead; d – dorsal, v – ventral; representative images colour-coded by depth).

distribution in animals without blood flow being similar in the CV but altered in ISVs (Fig. 4M, N and O).

Together, this suggested that vascular growth patterns in the trunk were unaltered, but remodelling, including intussusception, were lacking and that this is accompanied by changes in EC numbers and distribution.
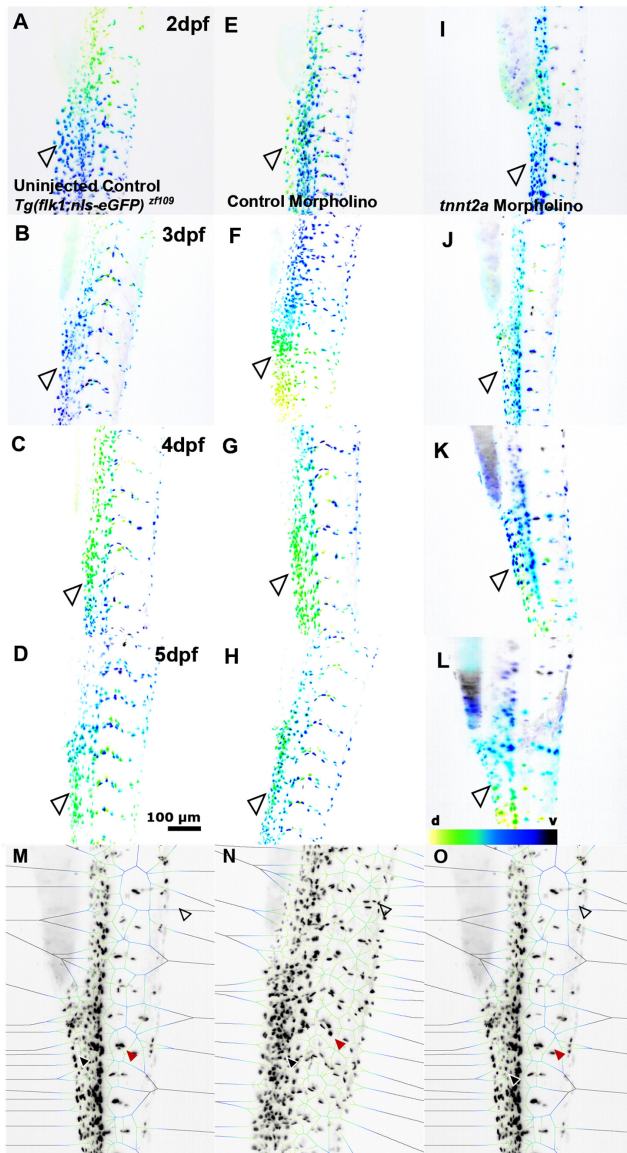
Lack of blood flow affects vascular area and EC number

To elucidate the effect of absent blood flow over time, we quantified cerebrovascular area (vascular voxels in 2D (MIPs)). This was significantly reduced in *tnnt2a* morphants from 2 to 5dpf (Fig. 5A; uninjected control

Figure 4
Lack of blood flow impacts trunk EC number. (A, B, C and D) Trunk EC
nuclei from 2 to 5dpf in *Tg(flk1:nls-eGFP)^zf109* uninjected control. (E, F, G and
H) Trunk EC nuclei in control MO. (I, J, K and L) Trunk EC nuclei in *tnnt2a*
MO (*n* = 7–10; two experimental repeats). Visual comparison of trunk EC
nuclei suggests comparable numbers between treatment groups
(d – dorsal, v – ventral; representative images colour-coded by depth).
(M, N and O) Voronoi analysis of trunk EC nuclei shows EC distribution is
maintained in the CV (black arrowhead), a decrease is observed in ISVs
(red arrowhead), and significant changes are observed more anteriorly
(unfilled arrowhead).

2dpf *P* < 0.0001, 3dpf *P* < 0.0001, 4dpf *P* < 0.0001, 5dpf
P < 0.0001), with similar results in craniovascular branch
points (Supplementary Fig. 3A). Similarly, the number
of cerebral EC nuclei was significantly reduced in *tnnt2a*

morphants from 2 to 5dpf; while EC number almost
doubled from 2 to 5dpf in controls, EC numbers were
almost unaltered in fish without blood flow (Fig. 5B;
uninjected control 2dpf *P*=0.0409, 3dpf *P* < 0.0001, 4dpf
P < 0.0001, 5dpf *P* < 0.0001). To examine the relationship
between vascular area and EC nuclei number, vascular
area-to-nuclei ratios were calculated (Fig. 5E), showing a
decrease in uninjected controls (0.78-fold-change 2–5dpf)
and control MO (0.87-fold-change 2–5dpf), while the ratio
increased in *tnnt2a* MO (1.69-fold-change 2–5dpf). This
showed that the number of nuclei-to-vasculature increased
in controls but decreased in animals without blood flow.

We performed the same analysis on the trunk, and
found that vascular area was significantly reduced by
absent blood flow at 2dpf (*P*=0.0074) and 3dpf (*P*=0.0195),
but not 4dpf (*P*=0.1904) and 5dpf (*P* > 0.9999) in *tnnt2a*
MO (Fig. 5C). Additionally, the number of nuclei was not
significantly lower at 2dpf (*P*=0.1514; Fig. 5D) but was
significantly decreased at 3–5dpf (3dpf *P*=0.0018, 4dpf
P=0.0013, 5dpf *P* < 0.0001). Similar results were observed
when assessing trunk vascular branch points as co-metric
(Supplementary Fig. 3B). Analysis of vascular-to-nuclei
ratio showed that vascular area increased in all three
groups (Fig. 5F; fold-change 2–5dpf: uninjected control
1.10, control MO 1.55, *tnnt2a* MO 2.51). Together, this
suggested that cerebral vessels were more severely affected
than trunk vessels by the absence of blood flow and that
lack of blood flow increases the vascular-to-nuclei ratio in
both the brain and trunk.

We next quantified the nuclei nearest neighbour
distance (NND), finding it to be decreased in *tnnt2a* MO in
both vascular beds (Fig. 5G and H), supporting the visual
assessment of Voronoi diagrams and previous studies that
suggest the less net distance between ECs in the absence of
flow (56).

To assess how the observed reduced head size
(Supplementary Fig. 4A) related to vascular and nuclei
density, vasculature-to-ROI and nuclei-to-ROI ratios were
quantified. This showed that for all three groups, vascular
coverage was maintained at about 30% from 2 to 5dpf
(Supplementary Fig. 4B), with ratios higher in *tnnt2a* MO
at 5dpf in comparison to uninjected controls (*P*=0.0074).
Similarly, the nuclei-to-ROI ratios were maintained over
time in all three groups (Supplementary Fig. 4C), but with
higher ratios in *tnnt2a* MO than in controls.

Together, this showed that even though *tnnt2a* MO
have a reduced head size, vasculature-to-ROI and nuclei-to-
ROI ratios are maintained or even larger than in controls.

© 2020 The authors
Published by Bioscientifica Ltd
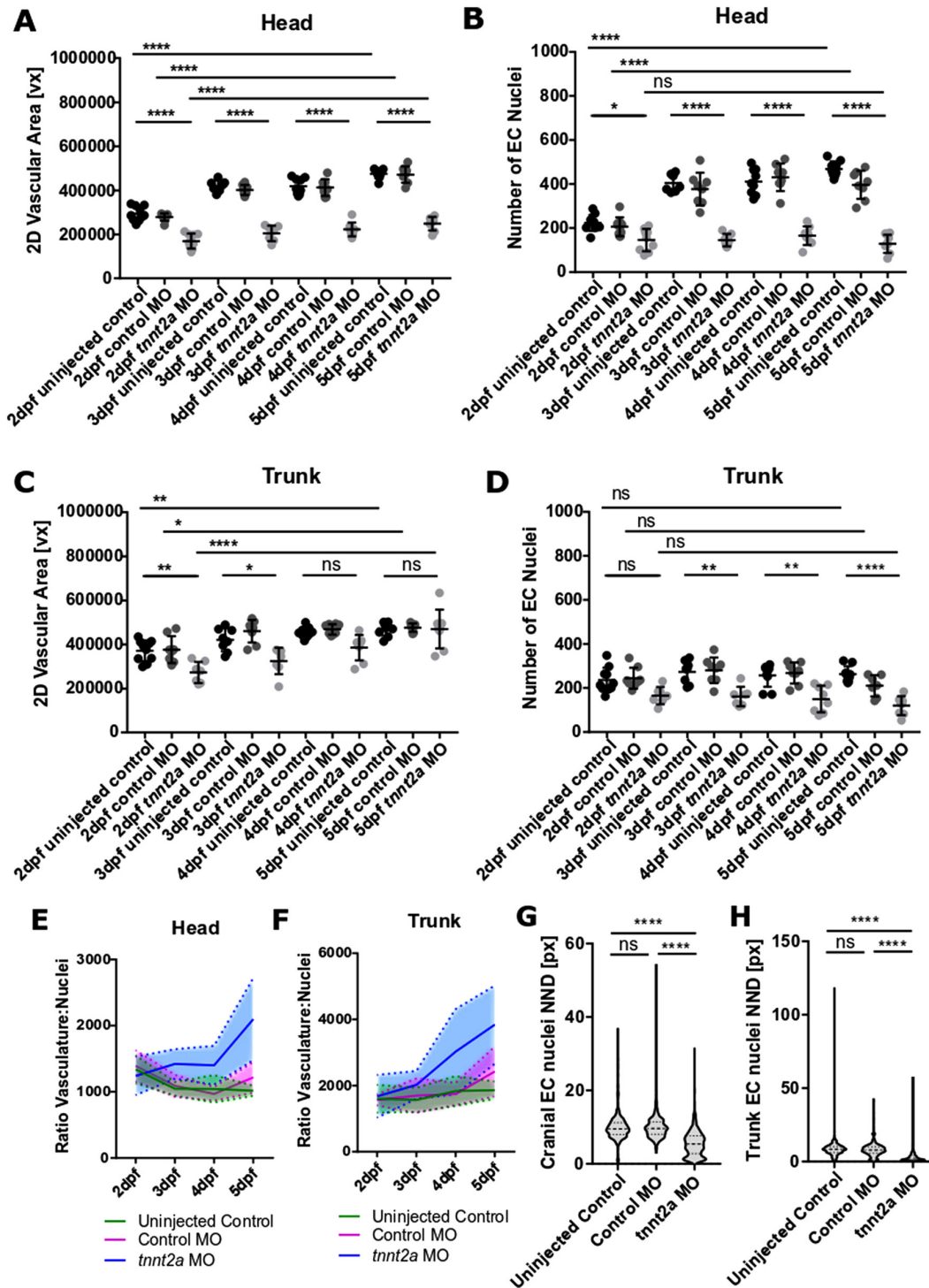
Figure 5

Quantification of vasculature and nuclei. (A) The cerebral vasculature is reduced in *tnnt2a* MO from 2 to 5dpf (*n* = 7– 10; two experimental repeats). (B) The number of cerebral EC nuclei is reduced in *tnnt2a* MO from 2 to 5dpf. (C) The trunk vasculature is reduced in *tnnt2a* MO at 2–3dpf, but not 4–5dpf (*n* = 7– 10; two experimental repeats). (D) The number of trunk EC nuclei is not altered in *tnnt2a* MO at 2dpf, but significantly reduced from 3 to 5dpf. (E) The ratio of cerebral vasculature-to-nuclei remains consistent in uninjected controls (green) and control MO (magenta), but increases over time in *tnnt2a* MO (blue). (F) The ratio of trunk vasculature-to-nuclei remains consistent in uninjected controls (green) and control MO (magenta), but increases over time in *tnnt2a* MO (blue). (G) Quantification of cerebral nuclei nearest neighbour distance (NND) showed nuclei distance to be decreased in *tnnt2a* MO in comparison to uninjected controls (*P* < 0.0001) and control MO (*P* < 0.0001; Kruskal–Wallis test). (H) Quantification of trunk nuclei NND showed nuclei distance to be decreased in *tnnt2a* MO in comparison to uninjected controls (*P* < 0.0001) and control MO (*P* < 0.0001; Kruskal–Wallis test).

Arterial and venous responses to lack of blood flow are vascular bed dependent

To study whether vessels of different identities were differentially or similarly impacted by lack of blood, we quantified the diameter of selected arteries and veins in the brain and trunk 3dpf. Quantification of cerebral BA diameter showed no difference between *tnnt2a* MO and controls (Supplementary Fig. 5A; uninjected control $P > 0.9999$, control MO $P > 0.9999$), while the diameter of the posterior cerebral vein (PCeV) was reduced in animals without blood flow (Supplementary Fig. 5B; uninjected control $P = 0.0175$,

control MO $P = 0.1230$). BA diameter was reduced by 2.5% (uninjected control 16.41 µm; *tnnt2a* MO 16.00 µm), while the PCeV diameter was reduced by 36.46% (uninjected control 11.52 µm; *tnnt2a* MO 7.32 µm). Quantifying trunk ISV diameters, aISV diameter (Supplementary Fig. 5C; uninjected control $P = 0.0017$, control MO $P = 0.0121$) and vISV diameter (Supplementary Fig. 5D; uninjected control $P = 0.0010$, control MO $P = 0.0094$) were both reduced in *tnnt2a* MO. The mean diameter of aISVs was reduced by 40.4% (uninjected control 10.52 µm; *tnnt2a* MO 6.27 µm), while the mean diameter of vISVs was reduced
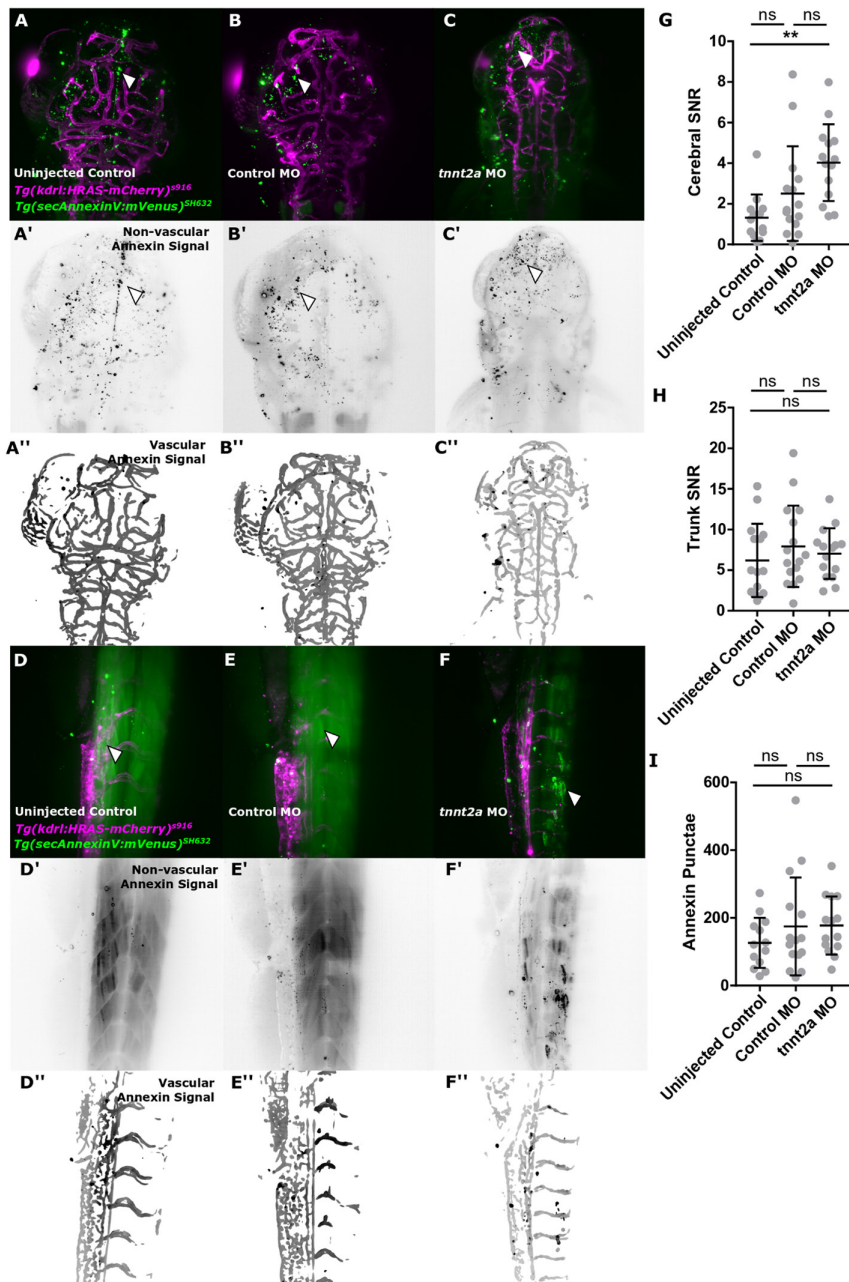
Figure 6

Cell death is increased by absent blood flow. (A, B and C) Cell death, visualized in the transgenic reporter line *Tg(secAnnexinV:mVenus)SH632* (*n* = 13–15; three experimental repeats; 3dpf). (D, E and F) Annexin levels in the trunk vasculature appeared visually similar between groups. (G) Quantification of cerebral annexin SNR showed an increase in *tnnt2a* MO in comparison to uninjected controls (*P* = 0.0012) but not control MO (*P* = 0.072; Kruskal–Wallis test). (H) Quantification of trunk annexin SNR showed no increase in *tnnt2a* MO in comparison to uninjected controls (*P* > 0.9999) or control MO (*P* > 0.9999; Kruskal–Wallis test). (I) Quantification of cerebral annexin foci (white arrowheads) showed no increase in *tnnt2a* MO in comparison to uninjected controls (*P* > 0.9999) and control MO (*P* = 0.4542; Kruskal–Wallis test).

by 46.64% (uninjected control 11 μm; *tnnt2a* MO 5.87 μm). The diameter of the DA (Supplementary Fig. 5E; uninjected control $P = 0.0008$, control MO $P = 0.0105$) as well as the posterior cardinal vein (PCV) (Supplementary Fig. 5F; uninjected control $P = 0.0159$, control MO $P = 0.0548$) were reduced in *tnnt2a* MO. The mean diameter of the DA was reduced by 40.76% (uninjected control 25.86 μm; *tnnt2a* MO 15.32 μm), while the mean diameter of the PCV was reduced by 29.1% (uninjected control 27.46 μm; *tnnt2a* MO 19.47 μm). This suggested that vessel diameter is impacted by flow in the vessel of venous and arterial identity in the trunk, while arterial vessel calibre of the BA is unaltered without flow.

To further examine whether EC number was affected by vessel identity and/or vascular bed, EC nuclei per vessel were quantified. Analysis of nuclei of cerebral BA and PCeV in 80 μm ROI showed no significant difference between those vessels in the examined treatment groups and no significant change upon lack of blood flow (Supplementary Fig. 5G). Quantification of nuclei in trunk aISV and vISV showed no significant difference in EC numbers between vessels of different identity (Supplementary Fig. 5H). Upon lack of blood flow arterial EC number was not reduced ($P = 0.5756$), but venous EC number was significantly reduced ($P = 0.0005$).

Together, this suggests that vascular responses are vascular-bed as well as vascular-identity specific.

Non-EC-specific cell death is increased by absent blood flow

To examine whether cell death contributed to the reduced EC numbers observed in *tnnt2a* morphants, we quantified this using the transgenic *Tg(secAnnexinV:mVenus)SH632* and the live dye Acridine Orange.

Visual inspection of the transgenic reporter line suggested an overall increase in cell death in *tnnt2a* MO compared to controls in the head (Fig. 6A, B and C) but not trunk (Fig. 6D, E and F), with specific foci found in the brain (white arrowhead). To examine whether the observed increase in annexin levels was vascular or non-vascular, we extracted non-vascular (Fig. 6A′, B′, C′, D′, E′ and F′) from vascular (Fig. 6A″, B″, C″, D″, E″ and F″) signal by producing vascular masks in 3D, finding that the observed cell death was not EC-specific. Quantification of tissue signal-to-noise ratio (SNR; Fig. 6G and H) showed an increase in the head in *tnnt2a* MO compared with uninjected controls ($P = 0.0012$, Fig. 6G) but not trunk ($P > 0.9999$, Fig. 6H). The number of annexin foci was not increased in *tnnt2a* MO (Fig. 6I; uninjected control $P > 0.9999$).

To examine this further, the same experiments were conducted using the live dye Acridine orange, which showed similar results. However, cell death foci were clearly increased in fish without blood flow using the Acridine Orange assay (Supplementary Fig. 6).

Together, this suggests that overall cell death is increased in *tnnt2a* MO, not restricted to EC.

Inflammatory responses are not triggered by the absence of blood flow

We next examined whether immune cell numbers would be altered due to the observed cell death potentially triggering an inflammatory response, or local tissue ischemia due to lack of blood flow, equally triggering an inflammatory response (58). As the observed effects of lack of blood flow were more severe in the head vasculature, quantification was only performed in this vascular bed.

Quantification of the number of macrophages in controls and *tnnt2a* MO at 3dpf (Fig. 7A, B and C) showed no difference between groups (Fig. 7D; $P = 0.2356$). Similarly, no difference was found in intracranial neutrophil numbers at 3dpf when comparing *tnnt2a* MO to controls (Fig. 7E, F and G; $P = 0.1708$).

To further examine whether the observed cell death was associated with altered tissue inflammation in the absence of altered macrophage and neutrophil numbers, we visualised the inflammatory mediator nitric oxide (NO) using the live dye DAF-FM. The visual assessment showed no difference in DAF-FM levels in the head (Fig. 8A, B and C) and trunk (Fig. D, E and F). This was confirmed by SNR quantification in the head (Fig. 8G; $P = 0.7967$) and trunk (Fig. 8H; $P = 0.9371$) which showed no differences comparing samples with blood flow to samples without blood flow.

Interestingly, we observed that the DAF-FM signal, previously described to be localized in the bulbus arteriosus after 2dpf (59), was absent in fish without blood flow (Supplementary Fig. 7), suggesting bulbus arteriosus NO expression is blood flow-dependent.

Together, our data suggested that the lack of blood flow does increase cell death but not tissue inflammation or immune cell recruitment at the investigated time-point.

Sprouting angiogenesis is altered but not halted by lack of blood flow

We next examined whether the observed changes in vascular patterning were due to changes in angiogenic
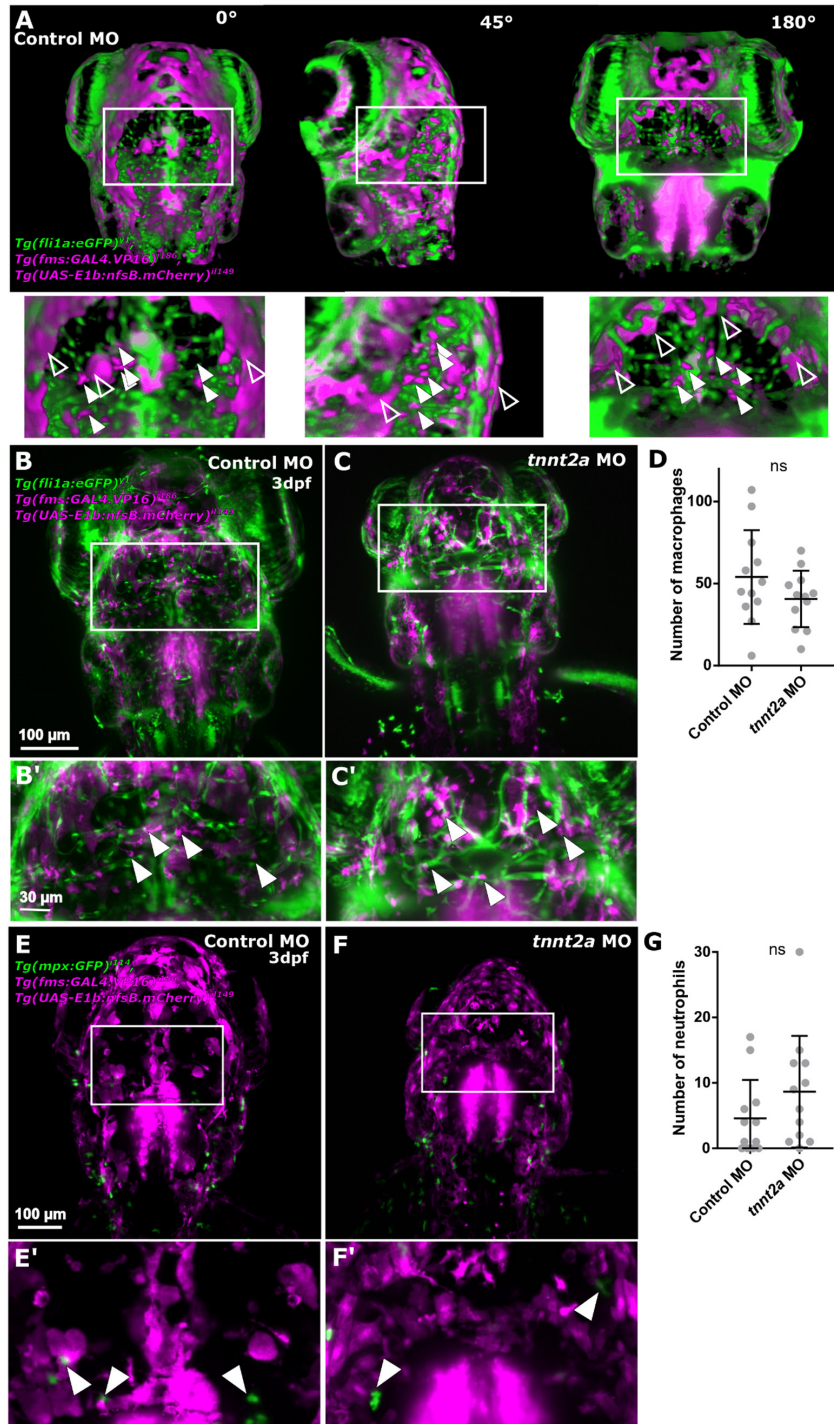
Figure 7

Lack of blood flow does not impact the number of cerebral innate immune cells. (A) Identification of immune cells was performed in 3D, allowing to discern non-specific signal (unfilled arrowhead) from immune cells (filled arrowhead). (B and C) Macrophages (magenta) were quantified examining the transgenic *Tg(fli1a:eGFP)^{y1}, Tg(fms:GAL4.VP16)^{i186}, Tg(UAS-E1b:nfsb.mCherry)^{il149}*. (D) Number of macrophages was not changed upon blood flow loss ($P = 0.2356$; $n = 12$; 3dpf; Mann–Whitney U test). (E and F) Neutrophils (green) were examined in the transgenic reporter line *Tg(mpx:GFP)^{i114}, Tg(fms:GAL4.VP16)^{i186}, Tg(UAS-E1b:nfsb.mCherry)^{il149}*. (G) Number of neutrophils was not changed upon blood flow loss ($P = 0.1708$; $n = 12$; two experimental repeats; 3dpf; Mann–Whitney U test).
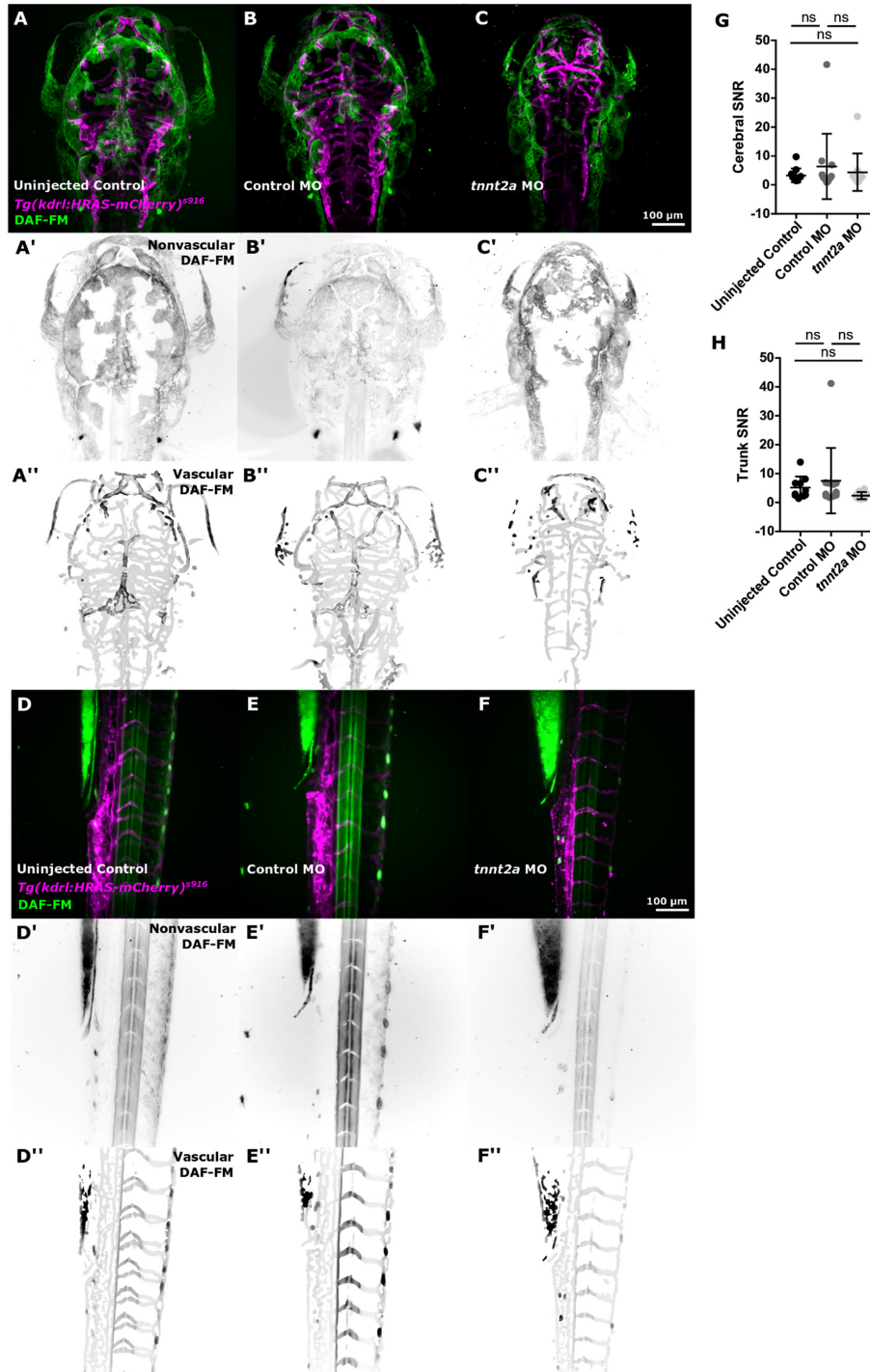
Figure 8

Inflammation is not increased by absent blood flow. (A, B and C) Examining nitric oxide (NO; visualized by DAF-FM) as an inflammatory marker, showed similar levels of NO in the head of uninjected controls, control MO, and *tnnt2a* MO (uninjected control $n = 11$, control MO $n = 12$, *tnnt2a* MO $n = 11$; three experimental repeats; 3dpf). (D, E and F) DAF-FM levels in the trunk vasculature appeared visually similar between groups. (G) Quantification of cerebral DAF-FM SNR showed no difference between *tnnt2a* MO and uninjected controls ($P > 0.9999$) or control MO ($P > 0.9999$; Kruskal–Wallis test). (H) Quantification of trunk DAF-FM SNR showed no difference between *tnnt2a* MO and uninjected controls ($P = 0.1391$) or control MO ($P = 0.1216$; Kruskal–Wallis test).

sprouting. To examine this, we first examined trunk ISV sprouting and subsequent dorsal longitudinal anastomotic vessel (DLAV) formation, which are known to develop in a highly stereotypic anterior-to-posterior growth pattern. Comparison of time-lapse data in controls and embryos without blood flow (Supplementary Fig. 8A), showed that ISVs are competent to sprout in fish with blood flow, as previously suggested (17). Also in agreement with previous studies, we did not observe inverse membrane blebbing to occur in the absence of flow (60). However,DLAV anastomosis is delayed in fish without flow. Following the initial delay, ISVs sprout laterally to form the DLAV upon anastomosis. While vessels in controls become subsequently perfused upon anastomosis, this is not the case in fish without blood flow.

We next examined cerebrovascular sprouting by examining CtA sprouting and numbers, due to their stereotypic sprouting pattern from the PHBC and anastomosis with the BA. This showed that CtA's were able to sprout from the PHBC and merge with the BA (Supplementary Fig. 8B) and when quantifying the number of sprouts this showed no significant difference in sprout number in fish without blood flow (Supplementary Fig. 8C; uninjected controls $P = 0.4737$). However, quantification of CtA's merged to the BA, were significantly reduced in the absence of blood flow (Supplementary Fig. 8D; uninjected controls $P = 0.0005$).

Importantly, for all examined vessels stereotypic patterning was observed in the absence of flow, suggesting that path-finding is dependent on factors other than blood flow.

Discussion

In this study, we present the first assessment of the impact of blood flow on zebrafish embryonic vascular development from 2 to 5dpf, and present the first comparison of the impact of flow in two vascular beds, namely the head and trunk. We show that though the overall response to lack of blood flow is similar in both vascular beds, the head vasculature is more severely impacted than trunk vasculature, with intra-cerebral vessels particularly being affected. Additionally, the effect of absent blood flow increases over time. Our data show that lack of blood flow significantly increases cell death without significant cell death in ECs, without evidence of a significant increase of tissue inflammation, as quantified by cerebral immune cell numbers and nitric oxide (Table 1).

Our work complements previous work (33), which found blood flow cessation to induce EC apoptosis in zebrafish embryos at 30hpf, while our assessment of cerebral macrophage numbers extends the examinations of Xu *et al.* who limited their studies to macrophage of the tectum (61). Our finding that NO is lacking in the bulbus arteriosus at 3dpf in fish without blood flow is the first functional evidence of bulbus arteriosus NO to be blood flow-dependent (59).

Our data showed that even in the complete absence of flow, stereotypic vascular patterning is preserved in the trunk and peripheral cerebral vessels. Our findings show that sprouting angiogenesis occurs in both vascular beds in the absence of flow but that anastomosis is delayed in the trunk and reduced in the head. This shows that in both, the trunk and head vasculature, vascular sprouting and path-seeking can occur in the absence of flow and is therefore not solely dependent on pressure gradients but likely to be induced by molecular or biochemical cues. However, successful fusion and anastomosis are blood flow dependent in both examined vascular beds. In agreement with previous work, we find that vascular plexus remodelling (56, 57) and vascular lumenization are blood flow-dependent (60). While previous studies suggest that pruning is directly driven by blood flow (19), it was never shown that this is the case for vessels that have never experienced blood flow. Our data show that early vascular networks are established. We suggest that, particularly in the head, multiple mechanisms contribute to the altered vascularization (a) lacking vascular self-fusion and remodelling in the absence of flow could be

Table 1 Overview of vascular properties altered upon lack of blood flow.

	Without blood flow	
	Head	Trunk
Vasculogenesis	Yes	Yes
Angiogenic sprouts	Yes	Yes
Anastomosis	Reduced	Delayed
Inverse membrane blebbing	N/A	No
Kugeln	No	N/A
Cell death	Increased	No
Macrophages and neutrophils	No	N/A
DAF-FM	No	No
Vascular area	Reduced	Reduced
EC number	Reduced	Reduced
Vasculature:nuclei ratio	Increased	Increased
NND	Reduced	Reduced
BP	Reduced	Reduced
Artery diameter	No	Reduced
Vein diameter	Reduced	Reduced
Artery nuclei	No	No
Vein nuclei	No	Reduced

the mechanism for the observed phenotype, as suggested for the subintestinal vein (23); (b) reduced vascular stabilization (62, 63); (c) potentially changed EC polarity and maintenance needs to be examined (18).

Critically, our work shows that vessel identity affects cell response to flow and that this is furthermore impacted by the vascular bed. Thus, we suggest that even though genetic factors establish vascular identity prior to blood flow (64, 65), the fine-tuning of vascular response is likely to be caused by extrinsic vascular-bed-specific signaling molecules or biochemical cues (7).

Our data show that EC nuclei net distance is reduced in the absence of flow by examination of NND and Voronoi tessellation. Our study suggests that this might be in part due to a reduced vascular area (i.e. vasculature and nuclei numbers are reduced; vascular-to-nuclei ratios are unaltered in early development but changed with age) rather than significantly altered cell movements as nuclei are observed in all formed vessels. However, it has been previously shown that ECs migrate against the flow, thus the lack of blood flow might also alter EC net distance via migration changes (66).

Our studies show that cerebral EC cell numbers double from 2 to 5dpf in controls but remain stationary in fish without blood flow. Even though we observe cell death, there is a high likelihood that decreased proliferation due to the lack of blood flow is a contributing factor (67).

Once established blood vessels are established, also their EC properties and functions rely on blood flow, as it was previously shown regarding maintenance (7, 62, 63, 68), polarity (66, 69), and *kugeln* (9).

The finding that central cerebral vessels show severely altered growth patterns, while peripheral vessels are less impacted, suggests that the response to blood flow is different in different vascular territories; whether this is due to a difference in vessel formation (e.g. peripheral vessels are formed from angiogenesis-derived clusters, while central vessels are formed by angiogenesis from primary vessels) (70, 71) or identity (e.g. perineural, extra-cerebral, vs intra-cerebral) (72) requires future investigation.

The mechanisms of the observed effects in response to absent blood flow still require future investigation. This could include examining the expression of different mechanoreceptors and EC properties to complement previous findings about the importance and impact of blood flow (32, 73, 74, 75, 76, 77). Similarly, molecular pathways and their context-dependent interpretation (such as VEGF, BMPs, Wnt (62, 78, 79, 80)) might play a role in encountered differences in the head and trunk vasculature.

Together, our findings emphasize the important role of blood flow in vascular patterning and development and highlight different responses in different vascular territories to mechanical stimuli.

Key points

- We here use zebrafish as a model to quantitatively assess the impact of the lack of blood flow in development and compare its impact in two vascular beds, namely the cerebral to trunk vasculature.
- In both vascular beds, vascular growth and endothelial cell number are reduced by lack of blood flow, with increasing effect size from 2–5 days post fertilization.
- Examination of vascular patterning shows that while in the absence of flow vasculogenesis and sprouting occur, anastomosis is delayed in the trunk and reduced in the head.
- Studying differential responses in vessel types, we found that vascular responses to absent blood flow are vascular-bed as well as vascular-identity specific.
- We found non-EC-specific cell death to be increased in both vascular beds, with a larger effect size in the brain, but that this cell death occurs without triggering recruitment of immune cells (macrophages or neutrophils) or tissue inflammation.

Declaration of interest

Timothy Chico is an Editorial Board Member of Vascular Biology. Timothy Chico was not involved in the review or editorial process for this paper, on which he is listed as an author. The other authors declare that they have no conflict of interest.

References

1 Demir R, Yaba A & Huppertz B. Vasculogenesis and angiogenesis in the endometrium during menstrual cycle and implantation. *Acta Histochemica* 2010 **112** 203–214. (https://doi.org/10.1016/j.acthis.2009.04.004)

2 Jung S & Kleinheinz J. Angiogenesis – the key to regeneration. In *Regenerative Medicine and Tissue Engineering*, pp. 443–472, 2013. (https://doi.org/10.5772/55542)

3 Singer AJ & Clark RAF. Cutaneous wound healing. *New England Journal of Medicine* 1999 **341** 738–746. (https://doi.org/10.1056/NEJM199909023411006)

4 Feigin VL, Norrving B & Mensah GA. Global burden of stroke. *Circulation Research* 2017 **120** 439–448. (https://doi.org/10.1161/CIRCRESAHA.116.308413)

5 Lackland DT & Weber MA. Global burden of cardiovascular disease and stroke: hypertension at the core. *Canadian Journal of Cardiology* 2015 **31** 569–571. (https://doi.org/10.1016/j.cjca.2015.01.009)

6 Abbott NJ, Patabendige AAK, Dolman DEM, Yusof SR & Begley DJ. Structure and function of the blood–brain barrier. *Neurobiology of Disease* 2010 **37** 13–25. (https://doi.org/10.1016/j.nbd.2009.07.030)

7 Chico TJA & Kugler EC. Cerebrovascular development: mechanisms and experimental approaches. *Cellular and Molecular Life Sciences* 2021 **78** 4377–4398. (https://doi.org/10.1007/s00018-021-03790-1)

8 Huntley MA, Bien-Ly N, Daneman R & Watts RJ. Dissecting gene expression at the blood-brain barrier. *Frontiers in Neuroscience* 2014 **8** 355. (https://doi.org/10.3389/fnins.2014.00355)

9 Kugler EC, van Lessen M, Daetwyler S, Chhabria K, Savage AM, Silva V, Plant K, MacDonald RB, Huisken J, Wilkinson RN, *et al.* Cerebrovascular endothelial cells form transient Notch-dependent cystic structures in zebrafish. *EMBO Reports* 2019 **20** e47047. (https://doi.org/10.15252/embr.201847047)

10 Vanlandewijck M, He L, Mäe MA, Andrae J, Ando K, Del Gaudio F, Nahar K, Lebouvier T, Laviña B, Gouveia L, *et al.* A molecular atlas of cell types and zonation in the brain vasculature. *Nature* 2018 **554** 475–480. (https://doi.org/10.1038/nature25739)

11 Bakkers J. Zebrafish as a model to study cardiac development and human cardiac disease. *Cardiovascular Research* 2011 **91** 279–288. (https://doi.org/10.1093/cvr/cvr098)

12 Chico TJA, Ingham PW & Crossman DC. Modeling cardiovascular disease in the zebrafish. *Trends in Cardiovascular Medicine* 2008 **18** 150–155. (https://doi.org/10.1016/j.tcm.2008.04.002)

13 Gut P, Reischauer S, Stainier DYR & Arnaout R. Little fish, big data: zebrafish as a model for cardiovascular and metabolic disease. *Physiological Reviews* 2017 **97** 889–938. (https://doi.org/10.1152/physrev.00038.2016)

14 Lawson ND & Weinstein BM. In vivo imaging of embryonic vascular development using transgenic zebrafish. *Developmental Biology* 2002 **248** 307–318. (https://doi.org/10.1006/dbio.2002.0711)

15 Huisken J, Swoger J, Del Bene F, Wittbrodt J & Stelzer EHK. Optical sectioning deep inside live embryos by selective plane illumination microscopy. *Science* 2004 **305** 1007–1009. (https://doi.org/10.1126/science.1100035)

16 Isogai S, Horiguchi M & Weinstein BM. The vascular anatomy of the developing zebrafish: an atlas of embryonic and early larval development. *Developmental Biology* 2001 **230** 278–301. (https://doi.org/10.1006/dbio.2000.9995)

17 Isogai S, Lawson ND, Torrealday S, Horiguchi M & Weinstein BM. Angiogenic network formation in the developing vertebrate trunk. *Development* 2003 **130** 5281–5290. (https://doi.org/10.1242/dev.00733)

18 Campinho P, Vilfan A & Vermot J. Blood flow forces in shaping the vascular system: a focus on endothelial cell behavior. *Frontiers in Physiology* 2020 **11** 552. (https://doi.org/10.3389/fphys.2020.00552)

19 Chen Q, Jiang L, Li C, Hu D, Bu JW, Cai D & Du JL. Haemodynamics-driven developmental pruning of brain vasculature in zebrafish. *PLoS Biology* 2012 **10** e1001374. (https://doi.org/10.1371/journal.pbio.1001374)

20 Hove JR, Koster RW, Forouhar AS, Acevedo-Bolton G, Fraser SE & Gharib M. Intracardiac fluid forces are an essential epigenetic factor for embryonic cardiogenesis. *Nature* 2003 **421** 172–177. (https://doi.org/10.1038/nature01282)

21 Kochhan E, Lenard A, Ellertsdottir E, Herwig L, Affolter M, Belting HG & Siekmann AF. Blood flow changes coincide with cellular rearrangements during blood vessel pruning in zebrafish embryos. *PLoS ONE* 2013 **8** e75060. (https://doi.org/10.1371/journal.pone.0075060)

22 Lee J, Fei P, Packard RRS, Kang H, Xu H, Baek KI, Jen N, Chen J, Yen H, Kuo CC, *et al.* 4-Dimensional light-sheet microscopy to elucidate shear stress modulation of cardiac trabeculation. *Journal of Clinical Investigation* 2016 **126** 1679–1690. (https://doi.org/10.1172/JCI83496)

23 Lenard A, Daetwyler S, Betz C, Ellertsdottir E, Belting HG, Huisken J & Affolter M. Endothelial cell self-fusion during vascular pruning. *PLoS Biology* 2015 **13** e1002126. (https://doi.org/10.1371/journal.pbio.1002126)

24 Ricard N & Simons M. When it is better to regress: dynamics of vascular pruning. *PLoS Biology* 2015 **13** e1002148. (https://doi.org/10.1371/journal.pbio.1002148)

25 Hoefer IE, den Adel B & Daemen MJAP. Biomechanical factors as triggers of vascular growth. *Cardiovascular Research* 2013 **99** 276–283. (https://doi.org/10.1093/cvr/cvt089)

26 Stainier DY & Fishman MC. The zebrafish as a model system to study cardiovascular development. *Trends in Cardiovascular Medicine* 1994 **4** 207–212. (https://doi.org/10.1016/1050-1738(94)90036-1)

27 Sehnert AJ & Stainier DYR. A window to the heart: can zebrafish mutants help us understand heart disease in humans? *Trends in Genetics* 2002 **18** 491–494. (https://doi.org/10.1016/s0168-9525(02)02766-x)

28 Sehnert AJ, Huq A, Weinstein BM, Walker C, Fishman M & Stainier DYR. Cardiac troponin T is essential in sarcomere assembly and cardiac contractility. *Nature Genetics* 2002 **31** 106–110. (https://doi.org/10.1038/ng875)

29 Stainier DYR, Raz E, Lawson ND, Ekker SC, Burdine RD, Eisen JS, Ingham PW, Schulte-Merker S, Yelon D, Weinstein BM, *et al.* Guidelines for morpholino use in zebrafish. *PLoS Genetics* 2017 **13** e1007000. (https://doi.org/10.1371/journal.pgen.1007000)

30 Fortuna V, Pardanaud L, Brunet I, Ola R, Ristori E, Santoro MM, Nicoli S & Eichmann A. Vascular mural cells promote noradrenergic differentiation of embryonic sympathetic neurons. *Cell Reports* 2015 **11** 1786–1796. (https://doi.org/10.1016/j.celrep.2015.05.028)

31 Rödel CJ, Otten C, Donat S, Lourenço M, Fischer D, Kuropka B, Paolini A, Freund C & Abdelilah-Seyfried S. Blood flow suppresses vascular anomalies in a zebrafish model of cerebral cavernous malformations. *Circulation Research* 2019 **125** e43–e54. (https://doi.org/10.1161/CIRCRESAHA.119.315076)

32 Watson O, Novodvorsky P, Gray C, Rothman AMK, Lawrie A, Crossman DC, Haase A, McMahon K, Gering M, Van Eeden FJ, *et al.* Blood flow suppresses vascular Notch signalling via dll4 and is required for angiogenesis in response to hypoxic signalling. *Cardiovascular Research* 2013 **100** 252–261. (https://doi.org/10.1093/cvr/cvt170)

33 Serbanovic-Canic J, de Luca A, Warboys C, Ferreira PF, Luong LA, Hsiao S, Gauci I, Mahmoud M, Feng S, Souilhol C, *et al.* Zebrafish model for functional screening of flow-responsive genes. *Arteriosclerosis, Thrombosis, and Vascular Biology* 2017 **37** 130–143. (https://doi.org/10.1161/ATVBAHA.116.308502)

34 Aleström P, D'Angelo L, Midtlyng PJ, Schorderet DF, Schulte-Merker S, Sohm F & Warner S. Zebrafish: housing and husbandry recommendations. *Laboratory Animals* 2020 **54** 213–224. (https://doi.org/10.1177/0023677219869037)

35 Westerfield M. *The Zebrafish Book: A Guide for Laboratory Use of Zebrafish (Brachydanio rerio)*. University of Oregon Press, 1993.

36 Kimmel CB, Ballard WW, Kimmel SR, Ullmann B & Schilling TF. Stages of embryonic development of the zebrafish. *Developmental Dynamics* 1995 **203** 253–310. (https://doi.org/10.1002/aja.1002030302)

37 Chi NC, Shaw RM, De Val S, Kang G, Jan LY, Black BL & Stainier DYR. Foxn4 directly regulates tbx2b expression and atrioventricular canal formation. *Genes and Development* 2008 **22** 734–739. (https://doi.org/10.1101/gad.1629408)

38 Blum Y, Belting HG, Ellertsdottir E, Herwig L, Lüders F & Affolter M. Complex cell rearrangements during intersegmental vessel sprouting and vessel fusion in the zebrafish embryo. *Developmental Biology* 2008 **316** 312–322. (https://doi.org/10.1016/j.ydbio.2008.01.038)

39 Renshaw SA, Loynes CA, Trushell DMI, Elworthy S, Ingham PW & Whyte MKB. A transgenic zebrafish model of neutrophilic inflammation. *Blood* 2006 **108** 3976–3978. (https://doi.org/10.1182/blood-2006-05-024075)

40 Gray C, Loynes CA, Whyte MKB, Crossman DC, Renshaw SA & Chico TJA. Simultaneous intravital imaging of macrophage and neutrophil behaviour during inflammation using a novel transgenic zebrafish. *Thrombosis and Haemostasis* 2011 **105** 811–819. (https://doi.org/10.1160/TH10-08-0525)

41 Morsch M, Radford R, Lee A, Don EK, Badrock AP, Hall TE, Cole NJ & Chung R. In vivo characterization of microglial engulfment of dying neurons in the zebrafish spinal cord. *Frontiers in Cellular Neuroscience* 2015 **9** 321. (https://doi.org/10.3389/fncel.2015.00321)

42 Hamilton N, Rutherford HA, Petts JJ, Isles HM, Weber T, Henneke M, Gärtner J, Dunning MJ & Renshaw SA. The failure of microglia to digest developmental apoptotic cells contributes to the pathology of RNaseT2-deficient leukoencephalopathy. *Glia* 2020 **68** 1531–1545. (https://doi.org/10.1002/glia.23829)

43 Verduzco D & Amatruda JF. Analysis of cell proliferation, senescence and cell death in zebrafish embryos. *Methods in Cell Biology* 2011 **101** 19–38. (https://doi.org/10.1016/B978-0-12-387036-0.00002-5)

44 Zhang C, Li C, Jia X, Wang K, Tu Y, Wang R, Liu K, Lu T & He C. In vitro and in vivo anti-inflammatory effects of polyphyllin VII through downregulating MAPK and NF-κB pathways. *Molecules* 2019 **24** 875. (https://doi.org/10.3390/molecules24050875)

45 Kojima H, Nakatsubo N, Kikuchi K, Kawahara S, Kirino Y, Nagoshi H, Hirata Y & Nagano T. Detection and imaging of nitric oxide with novel fluorescent indicators: diaminofluoresceins. *Analytical Chemistry* 1998 **70** 2446–2453. (https://doi.org/10.1021/ac9801723)

46 Kugler E, Plant K, Chico T & Armitage P. Enhancement and segmentation workflow for the developing zebrafish vasculature. *Journal of Imaging* 2019 **5** 14. (https://doi.org/10.3390/jimaging5010014)

47 Gonzalez R & Woods R. *Digital Image Processing*. Pearson Prenctice Hall, 2018.

48 Lim J. *Two-Dimensional Signal and Image Processing*, pp. 469–476. Englewood Cliffs, NJ: Prentice Hall, 1990.

49 Sternberg SR. Biomedical image processing. *Computer* 1983 **16** 22–34. (https://doi.org/10.1109/MC.1983.1654163)

50 Burger W & Burge M. *Digital Image Processing*. London: Springer, 2008. (https://doi.org/10.1007/978-1-4471-6684-9)

51 Schindelin J, Arganda-Carreras I, Frise E, Kaynig V, Longair M, Pietzsch T, Preibisch S, Rueden C, Saalfeld S, Schmid B, *et al.* Fiji – an Open Source platform for biological image analysis. *Nature Methods* 2012 **9** 676–682. (https://doi.org/10.1038/nmeth.2019)

52 Otsu N. A threshold selection method from gray-level histograms. *IEEE Transactions on Systems, Man, and Cybernetics* 1979 **9** 62–66. (https://doi.org/10.1109/TSMC.1979.4310076)

53 Kugler E, Chico T & Armitage P. Image analysis in light sheet fluorescence microscopy images of transgenic zebrafish vascular development. In *Medical Image Understanding and Analysis. MIUA 2018*, pp. 343–353. Eds M Nixon, S Mahmoodi & R Zwiggelaar. Cham: Springer, 2018. (https://doi.org/10.1007/978-3-319-95921-4_32)

54 Kugler E, Chico T & Armitage PA. Validating segmentation of the zebrafish vasculature. In *Medical Image Understanding and Analysis*, pp. 270–281. Eds Y Zheng, BM Williams & K Chen. Cham: Springer International Publishing, 2020. (https://doi.org/10.1007/978-3-030-39343-4_23)

55 Kimura E, Isogai S & Hitomi J. Integration of vascular systems between the brain and spinal cord in zebrafish. *Developmental Biology* 2015 **406** 40–51. (https://doi.org/10.1016/j.ydbio.2015.07.015)

56 Goetz JG, Steed E, Ferreira RR, Roth S, Ramspacher C, Boselli F, Charvin G, Liebling M, Wyart C, Schwab Y, *et al.* Endothelial cilia mediate low flow sensing during zebrafish vascular development. *Cell Reports* 2014 **6** 799–808. (https://doi.org/10.1016/j.celrep.2014.01.032)

57 Karthik S, Djukic T, Kim JD, Zuber B, Makanya A, Odriozola A, Hlushchuk R, Filipovic N, Jin SW & Djonov V. Synergistic interaction of sprouting and intussusceptive angiogenesis during zebrafish caudal vein plexus development. *Scientific Reports* 2018 **8** 9840. (https://doi.org/10.1038/s41598-018-27791-6)

58 Eltzschig HK & Carmeliet P. Hypoxia and inflammation. *New England Journal of Medicine* 2011 **364** 656–665. (https://doi.org/10.1056/NEJMra0910283)

59 Grimes AC, Stadt HA, Shepherd IT & Kirby ML. Solving an enigma: arterial pole development in the zebrafish heart. *Developmental Biology* 2006 **290** 265–276. (https://doi.org/10.1016/j.ydbio.2005.11.042)

60 Gebala V, Collins R, Geudens I, Phng LK & Gerhardt H. Blood flow drives lumen formation by inverse membrane blebbing during angiogenesis in vivo. *Nature Cell Biology* 2016 **18** 443–450. (https://doi.org/10.1038/ncb3320)

61 Xu J, Wang T, Wu Y, Jin W & Wen Z. Microglia colonization of developing zebrafish midbrain is promoted by apoptotic neuron and lysophosphatidylcholine. *Developmental Cell* 2016 **38** 214–222. (https://doi.org/10.1016/j.devcel.2016.06.018)

62 Bussmann J, Wolfe SA & Siekmann AF. Arterial-venous network formation during brain vascularization involves hemodynamic regulation of chemokine signaling. *Development* 2011 **138** 1717–1726. (https://doi.org/10.1242/dev.059881)21429983.

63 Packham IM, Gray C, Heath PR, Hellewell PG, Ingham PW, Crossman DC, Milo M & Chico TJA. Microarray profiling reveals CXCR4a is downregulated by blood flow in vivo and mediates collateral formation in zebrafish embryos. *Physiological Genomics* 2009 **38** 319–327. (https://doi.org/10.1152/physiolgenomics.00049.2009)

64 Geudens I, Coxam B, Alt S, Gebala V, Vion AC, Meier K, Rosa A & Gerhardt H. Artery-vein specification in the zebrafish trunk is pre-patterned by heterogeneous Notch activity and balanced by flow-mediated fine-tuning. *Development* 2019 **146** dev181024. (https://doi.org/10.1242/dev.181024)

65 Weijts B, Gutierrez E, Saikin SK, Ablooglu AJ, Traver D, Groisman A & Tkachenko E. Blood flow-induced Notch activation and endothelial migration enable vascular remodeling in zebrafish embryos. *Nature Communications* 2018 **9** 5314. (https://doi.org/10.1038/s41467-018-07732-7)

66 Franco CA, Jones ML, Bernabeu MO, Vion AC, Barbacena P, Fan J, Mathivet T, Fonseca CG, Ragab A, Yamaguchi TP, *et al.* Non-canonical Wnt signalling modulates the endothelial shear stress flow sensor in vascular remodelling. *eLife* 2016 **5** e07727. (https://doi.org/10.7554/eLife.07727)

67 Bazmara H, Soltani M, Sefidgar M, Bazargan M, Mousavi Naeenian M & Rahmim A. The vital role of blood flow-induced proliferation and migration in capillary network formation in a multiscale model of angiogenesis. *PLoS ONE* 2015 **10** e0128878. (https://doi.org/10.1371/journal.pone.0128878)

68 Neto F, Klaus-Bergmann A, Ong YT, Alt S, Vion AC, Szymborska A, Carvalho JR, Hollfinger I, Bartels-Klein E, Franco CA, *et al.* YAP and TAZ regulate adherens junction dynamics and endothelial cell distribution during vascular development. *eLife* 2018 **7** e31037. (https://doi.org/10.7554/eLife.31037)

69 Kwon HB, Wang S, Helker CSM, Rasouli SJ, Maischein HM, Offermanns S, Herzog W & Stainier DYR. In vivo modulation of endothelial polarization by apelin receptor signalling. *Nature Communications* 2016 **7** 11805. (https://doi.org/10.1038/ncomms11805)

70 Proulx K, Lu A & Sumanas S. Cranial vasculature in zebrafish forms by angioblast cluster-derived angiogenesis. *Developmental Biology* 2010 **348** 34–46. (https://doi.org/10.1016/j.ydbio.2010.08.036)

71 Siekmann AF, Standley C, Fogarty KE, Wolfe SA & Lawson ND. Chemokine signaling guides regional patterning of the first embryonic artery. *Genes and Development* 2009 **23** 2272–2277. (https://doi.org/10.1101/gad.1813509)

72 Vanhollebeke B, Stone OA, Bostaille N, Cho C, Zhou Y, Maquet E, Gauquier A, Cabochette P, Fukuhara S, Mochizuki N, *et al.* Tip cell-specific requirement for an atypical Gpr124- and Reck-dependent Wnt/beta-catenin pathway during brain angiogenesis. *eLife* 2015 **4** e06489. (https://doi.org/10.7554/eLife.06489)

73 Feng S, Bowden N, Fragiadaki M, Souilhol C, Hsiao S, Mahmoud M, Allen S, Pirri D, Ayllon BT, Akhtar S, *et al.* Mechanical activation of hypoxia-inducible factor 1α drives endothelial dysfunction at atheroprone sites. *Arteriosclerosis, Thrombosis, and Vascular Biology* 2017 **37** 2087–2101. (https://doi.org/10.1161/ATVBAHA.117.309249)

74 Mahmoud MM, Serbanovic-Canic J, Feng S, Souilhol C, Xing R, Hsiao S, Mammoto A, Chen J, Ariaans M, Francis SE, *et al.* Shear stress induces endothelial-to-mesenchymal transition via the transcription factor Snail. *Scientific Reports* 2017 **7** 3375. (https://doi.org/10.1038/s41598-017-03532-z)

75 Novodvorsky P & Chico TJA. The role of the transcription factor KLF2 in vascular development and disease. *Progress in Molecular Biology and Translational Science* 2014 **124** 155–188. (https://doi.org/10.1016/B978-0-12-386930-2.00007-0)

76 Serbanovic-Canic J, Souilhol C & Evans PC. Shear stress makes its mark on the endothelial genome. *Cardiovascular Research* 2019 **115** 1449–1451. (https://doi.org/10.1093/cvr/cvz088)

77 Souilhol C, Serbanovic-Canic J, Fragiadaki M, Chico TJ, Ridger V, Roddie H & Evans PC. Endothelial responses to shear stress in atherosclerosis: a novel role for developmental genes. *Nature Reviews: Cardiology* 2020 **17** 52–63. (https://doi.org/10.1038/s41569-019-0239-5)

78 Benz F, Wichitnaowarat V, Lehmann M, Germano RF, Mihova D, Macas J, Adams RH, Taketo MM, Plate KH, Guérit S, *et al.* Low wnt/β-catenin signaling determines leaky vessels in the subfornical organ and affects water homeostasis in mice. *eLife* 2019 **8** e43818. (https://doi.org/10.7554/eLife.43818)

79 Liang D, Chang JR, Chin AJ, Smith A, Kelly C, Weinberg ES & Ge R. The role of vascular endothelial growth factor (VEGF) in vasculogenesis, angiogenesis, and hematopoiesis in zebrafish development. *Mechanisms of Development* 2001 **108** 29–43. (https://doi.org/10.1016/s0925-4773(01)00468-3)

80 Wiley DM & Jin SW. Bone morphogenetic protein functions as a context-dependent angiogenic cue in vertebrates. *Seminars in Cell and Developmental Biology* 2011 **22** 1012–1018. (https://doi.org/10.1016/j.semcdb.2011.10.005)